

# Geophysical Research Letters

## RESEARCH LETTER

10.1029/2019GL084719

### Key Points:

- Ps receiver functions detect temporal variations in subsurface properties due to groundwater recharge
- Temporal variations in autocorrelations of seismic noise are consistent with subsurface changes seen by receiver functions
- A simple physical model accurately predicts observed P- and S-wave velocity changes due to groundwater recharge

### Supporting Information:

- Supporting Information S1

### Correspondence to:

D. Kim,  
dk696@umd.edu

### Citation:

Kim, D., & Lekic, V. (2019). Groundwater variations from autocorrelation and receiver functions. *Geophysical Research Letters*, 46, 13,722–13,729. <https://doi.org/10.1029/2019GL084719>

Received 30 JUL 2019

Accepted 20 NOV 2019

Accepted article online 25 NOV 2019

Published online 3 DEC 2019

## Groundwater Variations From Autocorrelation and Receiver Functions

D. Kim<sup>1</sup> and V. Lekic<sup>1</sup>

<sup>1</sup>Department of Geology, University of Maryland, College Park, MD, USA

**Abstract** Using a 20-year continuous broadband record and two independent single-station techniques—ambient noise autocorrelation and receiver functions—we document a relationship between subsurface seismic response and groundwater levels (GWLs) in the Gulf Coast Aquifer System of southern Texas. We find that a surge of GWL following three consecutive hurricanes and documented at an adjacent monitoring well is accompanied with changes in receiver function power spectra and ambient noise autocorrelations. Using a simple physical model, we show that GWL changes should affect P- ( $V_p$ ) more strongly than S-wave ( $V_s$ ) velocities, consistent with our observations and previous ones based on inter-station correlations. Agreement between receiver function and ambient noise analyses shows that both can be used to reliably estimate temporal changes in subsurface properties on long timescales. Due to their sensitivity to  $V_p$ , single-station techniques respond more strongly to GWL changes, making them useful for characterizing and monitoring aquifer systems.

**Plain Language Summary** Even though groundwater in large aquifer systems is often relied upon as a water source, it is one of the least well-known components of the hydrologic cycle. Here, we document a relationship between ground vibrations recorded by a seismometer and the groundwater levels in the Gulf Coast Aquifer System of southern Texas. We find that a surge of groundwater level following three consecutive hurricanes is accompanied with changes in the characteristics of seismic vibrations set-up in the shallow subsurface. Characteristics of vibrations due to both ambient noise and from earthquake show similar signals. Using a simple physical model, we show how groundwater level changes the properties of the subsurface to explain the seismic observations. Our work illustrates how even a single seismometer can be used to monitor groundwater level changes, which is particularly useful in aquifer systems lacking monitoring wells, and can complement other geophysical measurements from gravity or uplift/subsidence sensed data from satellites.

## 1. Introduction

Sustainable water resource management is critical to global challenges such as climate change, energy generation, droughts, and food security. Groundwater in large aquifer systems is often relied upon as a water source, yet it is one of the least well-characterized components of the hydrologic cycle. Fortunately, in the United States, a national network of groundwater monitoring wells is operated by the United States Geological Survey (USGS) National Water Information System (U.S. Geological Survey, 2016). In many areas around the globe, however, groundwater attracts insufficient management attention compared to more visible surface water resources in rivers and reservoirs and is often poorly monitored (Famiglietti, 2014). In the absence of well data, extracting information about the distribution of groundwater and its spatiotemporal variations using geophysical techniques can be greatly beneficial, particularly in regions under water stress where groundwater is used as an additional water source (Wada et al., 2010).

Geodetic measurements can characterize how the Earth's crust responds to groundwater changes in both time and space. Gravity data can be used to infer changes in mass balance due to hydrological variations in regional- (e.g., Rodell et al., 2009) and local-scale aquifers (e.g., Chen et al., 2016; Rodell et al., 2007; Strassberg et al., 2007; Swenson et al., 2006; Yeh et al., 2006). Similarly, the temporal or spatial pattern of uplift and subsidence observed with remote sensing can be related to the deformational response resulting from groundwater variations. For example, Interferometric Synthetic Aperture Radar (InSAR) measurements of deformation have been used to infer changes in groundwater content (e.g., Amelung et al., 1999; Chaussard et al., 2017; Schmidt & Bürgmann, 2003). Global Positioning System (GPS) studies, on the

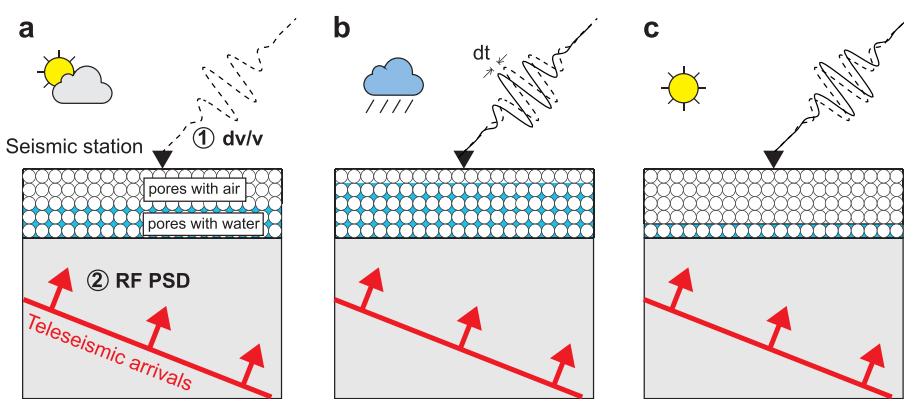


**Figure 1.** Conceptual diagrams depicting changes in GWL (blue) within an aquifer and the proposed seismic methods for detecting them. The uppermost layer in each panel indicates a schematic aquifer system with a constant porosity. Changes in the GWL can be monitored by measuring  $dv/v$  from ambient noise correlation (i.e., computing  $-dt/t$  from a dashed trace with a solid trace) and power spectral density (PSD) of receiver functions (RFs) from teleseismic arrivals (in red). NB: dashed/solid traces are reference/individual correlograms (waveforms), respectively.

other hand, have focused on investigating temporal changes in aquifer properties, including seasonal variations (e.g., Argus et al., 2014), drought (e.g., Borsa et al., 2014), and pumping (e.g., Amos et al., 2014; Huang et al., 2016). Despite their great utility, these geodetic and gravity techniques only constrain a depth-integrated quantity (i.e., mass and surface displacement), the interpretation of which is inherently nonunique. For example, infinitely many mass anomaly distributions can explain gravitational acceleration observations equally well (e.g., Blakely, 1995). Analogously, interpreting the depth distribution of groundwater changes from deformation patterns observed using InSAR or GPS on the surface suffers from significant trade-offs.

Seismic observations can provide more direct measurements about conditions in the subsurface. In order to monitor such active subsurface process using seismology, one needs a reproducible seismic signal propagating through the system. Controlled artificial sources have been successfully used for this purpose (e.g., Niu et al., 2008) especially in the petroleum production context (e.g., Silver et al., 2007), but small changes in subsurface properties due to external perturbations can also be monitored using seismic energy generated by earthquakes or ambient noise (e.g., Audet, 2010; Larose et al., 2015; Meier et al., 2010; Porritt & Yoshioka, 2017; Snieder & Page, 2007). Time-lapse monitoring can be performed across a range of timescales, from short ones associated with high precipitation events, through seasonal variations, to long-term changes due to groundwater extraction and drought. Some of the better known applications of monitoring temporal changes using seismic observations in the literature include glaciers (Mordret et al., 2016), volcanoes (e.g., Duputel et al., 2009; Sens-Schönfelder & Wegler, 2006), rivers (e.g., Schmandt et al., 2013; Tsai, 2011), groundwater (Sens-Schönfelder & Wegler, 2011; Clements & Denolle, 2018), active fault and landslide processes (e.g., Brenguier et al., 2008; Mainsant et al., 2012; Wegler & Sens-Schönfelder, 2007), infrastructure (e.g., Goodling et al., 2018; Mikael et al., 2013), and planetary targets (e.g., Duvall et al., 1993; Sens-Schönfelder & Larose, 2008).

Here, we demonstrate the feasibility of applying two well-known complementary seismic techniques for monitoring temporal variations in the seismic response of the subsurface, which we relate to groundwater level (GWL) changes (Figure 1). In the following sections, we show how seismic velocities can constrain changes on an inter-annual timescale and document the long-term stability of receiver function (RF) and autocorrelation estimates of subsurface velocities. We then propose a causal relationship between those observations and GWLs based on a simple physical model.

## 2. Data and Methods

Monitoring temporal variations in subsurface properties is based on comparing the seismic response of a subsurface structure in one time frame to its response in another. While initially performed using earthquake doublets, or a pair of microearthquakes (Poupinet et al., 1984), it is now more commonly

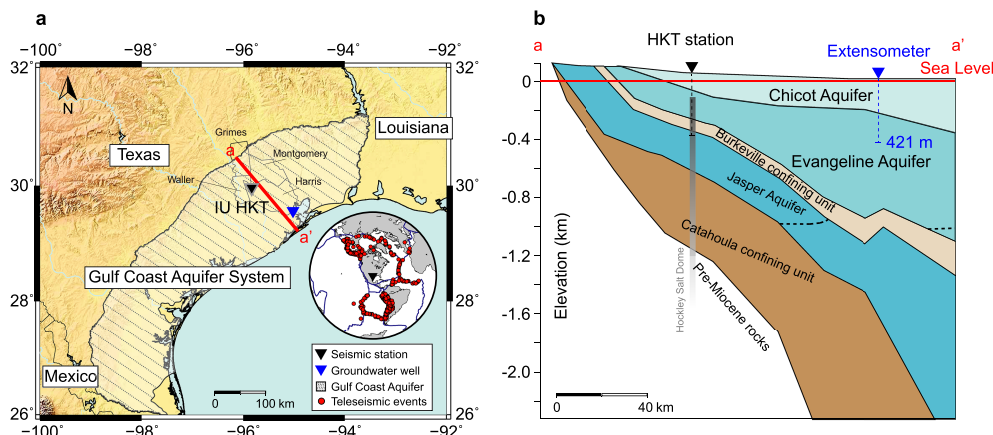


**Figure 2.** (a) Study area in the Gulf Coast Aquifer System (GCAS) of Texas. Both ambient noise and teleseismic RFs are computed using seismic recordings spanning 1995–2017 from IU.HKT station in Harris County, Texas (black triangle). Note that IU.HKT station is installed inside the Hockley salt dome (Deussen & Lane, 1925) indicated by gray outline. Groundwater level (GWL) measurements are from USGS Seabrook borehole extensometer in the Evangeline Aquifer (blue triangle). Red circles in the inset map are teleseismic earthquakes used in computing the RFs. (b) Cross section across the Gulf Coast Aquifer, corresponding to red line in (a). The dashed line indicates approximate down-dip limit of freshwater. NB: Vertical scale is greatly exaggerated (modified from Baker, 1979; Kasmarek & Robinson, 2004).

accomplished using ambient noise correlation (Shapiro et al., 2005), which allows the Earth's impulse response to be determined without earthquake recordings. For example, Sens-Schönfelder and Wegler (2006) constrained temporal variations by comparing daily inter-station correlations to a reference correlation (i.e., reference state of the system) obtained by averaging over a much larger period. Of particular relevance to our study is work relating changes in seismic velocity to groundwater recharge by precipitation (Sens-Schönfelder & Wegler, 2011) and a study showing that local variation of the GWL in the San Gabriel Valley, CA, can be tracked using the inter-station correlation of ambient noise (Clements & Denolle, 2018). To detect seismic velocity changes, we compute correlations of ambient noise signals at seismic stations and measure perturbations in subsurface velocity ( $dv/v$ ) using the “stretching” technique (Hadzioannou et al., 2009; Larose et al., 2015; Mordret et al., 2016). Small velocity perturbations delay or advance correlations in time and (traces in solid line, Figures 2b and 2c) decorrelate them from the reference state (traces in dashed line, Figure 2); we measure the stretching coefficient ( $dv/v$ ) that compensates the time delay ( $-dt/t$ ) to maximize the correlation with the reference state of the system. Our study differs from the previous ambient noise analysis in that we focus on a single-station approach using autocorrelation rather than the cross-correlation method. We obtain autocorrelations from both vertical and horizontal components.

In addition to ambient noise correlations, we use an independent, complementary method based on analyzing teleseismic waveforms to isolate waves scattered/converted directly beneath the receiver (method 2, Figure 2). This method, called RFs, removes complexities associated with earthquake rupture and source-side propagation using deconvolution, thereby isolating subreceiver structure (Burdick & Langston, 1977). Typical P-to-S teleseismic RFs are analyzed and filtered in a way that makes it difficult to resolve structures that are smaller than ~2 km (e.g., Kim et al., 2019); however, comparison with ground-truth well estimates show that high frequency RFs can constrain shallow structures at scales smaller than <500 m (Leahy et al., 2012). Furthermore, Audet (2010) showed that power spectral density (PSD) of RFs can even resolve temporal variations in crustal velocity structure following the 2004 Parkfield ( $M_w$  6) earthquake, constraining S-wave velocity changes of ~0.06 km/s. We analyze the spectrograms of RFs and exploit both amplitude and phase information of subsurface scattering/conversions contained in the RFs spectra.

Both ambient noise and teleseismic RFs are computed from broadband recordings spanning 1995–2017 at IU.HKT station in Harris County, Texas (Albuquerque Seismological Laboratory, 1988) installed above the Gulf Coast Aquifer System (GCAS) of southern Texas (dashed region, Figure 2a). For each component, we compute the autocorrelation of ambient noise records and measure the changes in seismic velocity with respect to a reference time period (supporting information Figure S1). To do so, instrument response

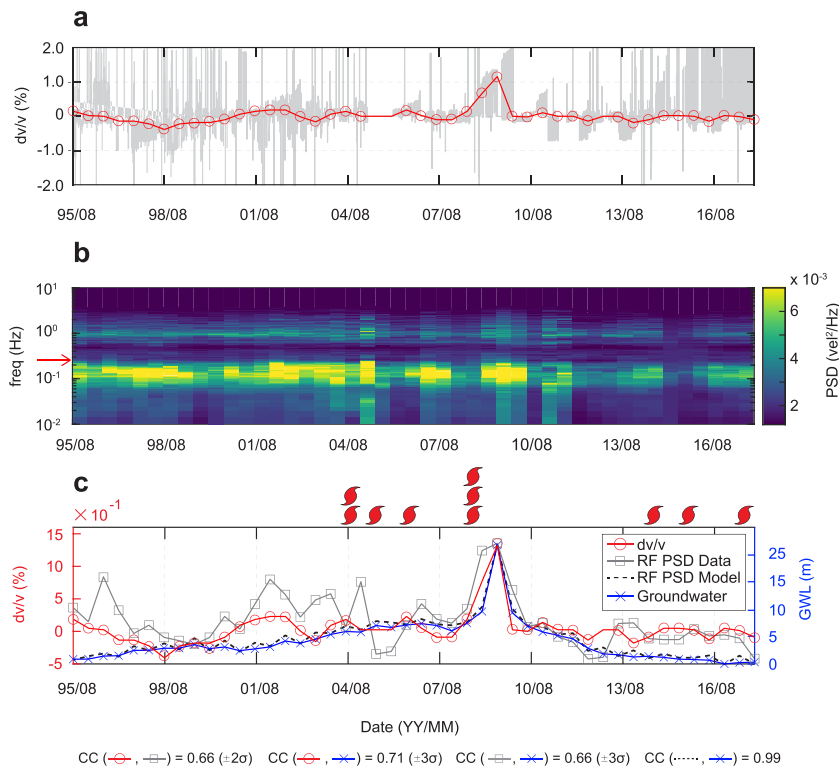


**Figure 3.** (a) Temporal variation in seismic velocity using ambient noise correlations. Apparent velocity changes computed based on daily autocorrelation of ambient noise recordings (gray line) and corresponding yearly average (red line) during 1995–2017 at IU.HKT station (Figure 2). (b) Temporal variations in PSD of RFs from 829 teleseismic earthquakes (inset, Figure 2) are binned in 50% overlapping, 12-month windows. (c) Comparison of observed GWL (blue line),  $dv/v$  (red circles), RF PSDs at 0.26–0.3 Hz (gray squares, red arrow at Figure 3b), and PSDs of synthetic RFs at 0.25–0.35 Hz (see Figure 4). Red symbols at the top indicate category 4 or larger hurricanes. The PSD of RFs is scaled to the  $dv/v$  measurement for easier visualization. Correlation between the two seismic measurements and groundwater data are shown at the bottom; all are significant above the 95% confidence level (see main text and Figure S3 for details).

removed data are demeaned, detrended, filtered between 0.01 and 8 Hz, and spectrally whitened. We apply 1-bit normalization and autocorrelate 6-min segments (with 50% overlapping window) from a daily record and compute phase-weighted stacks (Ventosa et al., 2017). Daily changes in seismic velocity (light gray lines) are found by grid search from  $-0.02$  to  $0.02$  of  $dv/v$  that maximizes the correlation coefficient between the stretch-applied autocorrelograms and the reference autocorrelation record.

To compute P-to-S RFs, three-component seismic recordings of teleseismic events are processed according to the procedure of Abt et al. (2010). We compute RFs (Figure S2) using an iterative time domain deconvolution (Ligorria & Ammon, 1999). The same filter used for ambient noise processing is also applied. A total of 829 teleseismic earthquakes with  $M_w > 5.5$  are used that repeatedly illuminate the same volume of crustal aquifer system quasi-continuously (inset, Figure 2a). Note that RFs can be easily biased by various levels of noise; horizontal components in particular are sensitive on short-term seasonal noise due to tilt thus dominant PSD in RF data (Audet, 2010). To effectively suppress such seasonal variations, RFs (Figure S2) are binned in moving, 50% overlapping, 12-month windows (Figure 3b).

Ambient noise and P-to-S RF analyses of data from the same seismic station provide independent constraints on variations in subsurface velocity. The inference made from seismic observations is compared against GWL measurements from USGS Seabrook borehole extensometer (Figures 2a and 2b). The depth of the well is 421 m below land surface and is completed in the Evangeline Aquifer in Harris County, TX (Kasmarek et al., 2012). Monthly GWL measurements are averaged in the same 12-month windows used for processing seismic data and detrended prior to the correlation analysis.

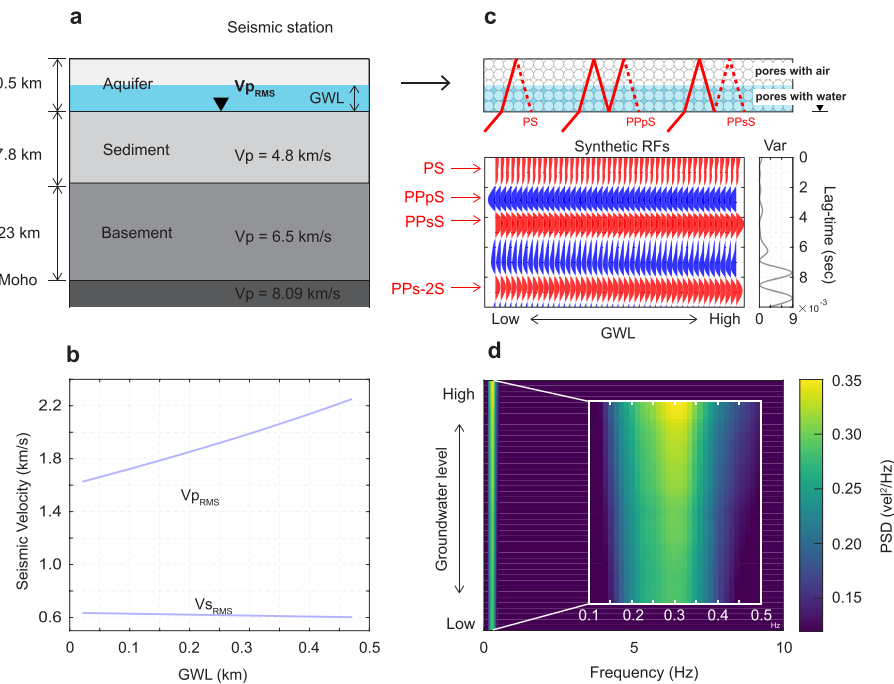


**Figure 4.** Physical model relating seismic velocities, synthetic RFs, and GWL for GCAS. (a) Velocity model used to generate synthetic RFs at IU.HKT station (Figure 2). The uppermost layer indicates GCAS of southern Texas. (b) Seismic velocities are estimated based on fluid substitution approach of Gassmann (1951) of water (blue) and air (white) in the pores from the background aquifer rock (top, Figure 4c). See Figure S5 for seismic velocity changes due to GWL variations calculated for a range of porosity between 0.1 and 0.4. GWL data of 1995–2017 (Figure 2) are normalized to 0–500 m to capture high and low aquifer scenarios of the model. (c) First 10 s of the synthetic RFs and their variance in amplitude as a function of lag-time. (d) Temporal variations in PSD of synthetic receiver functions showing strong frequency dependence.

### 3. Results and Discussion

We focus on analyzing a 23-year record of averaged  $dv/v$  measurements from vertical component autocorrelations, with the expectation that vertical component will be more sensitive to  $V_p$  than horizontal component autocorrelations. The largest increase in  $dv/v$  of 1.2% occurs during 2008–2010 (red line, Figures 3a and 3c). Although little correlation is observed between  $dv/v$  and PSD of RFs under its full bandwidth (Figure 3b), the strongest correlation between the two seismic measurements is found in the 0.26–0.3 Hz frequency range. We find that the GWL (blue, Figure 3c) and averaged  $dv/v$  (red, Figure 3c) track each other, with the GWL also reaching its maximum in the same 2008–2010 period. Moreover, GWL and PSD of RFs also correlate, with strongest correlation in the 0.67–0.71 Hz frequency range. The strong distinctive peak in GWL observed during 2008–2010, in particular, is consistent with the median PSD of RFs from this frequency range (gray, Figure 3c).

While abrupt changes in  $dv/v$  amplitudes have been reported after nearby earthquakes elsewhere (Brenguier et al., 2008; Wegler et al., 2009), the tectonic stability of the study area and paucity of seismicity makes such an explanation highly unlikely. Instead, we attribute the sudden increase observed in both  $dv/v$  and PSD of RFs to three consecutive hurricanes (i.e., Gustav, Ike, and Norbert; red symbols in Figures 3c and S1) that occurred less than a month apart prior to the observed peak during 2008–2010. We also note similar  $dv/v$  changes along with GWL rise in the San Gabriel Valley, CA, due to 1 m of total precipitation, the highest amount of rainfall in 100 years in Los Angeles (Clements & Denolle, 2018). However, we report the opposite sign of  $dv/v$  changes with one order of magnitude larger here in Texas and will provide a physical explanation for this difference later in the section.

To assess the statistical significance of the correlation between the measured GWL and variations in seismic  $dv/v$  and RF changes, we generate simulated time series with the same frequency content as observations but

random phase. By recomputing the correlation coefficients for 1,000 such randomly generated time series, we find that correlations among seismic observables and the GWL are statistically significant well above 2-sigma (Figures 3c and S3). Substantially lower correlation coefficients from both horizontal component measurements suggest the primary role of P-wave velocity changes (Figure S1). Similar analysis did not find any statistically significant correlation between seismic observables and precipitation in the region. These results show that single-station seismic data can potentially provide constraints on GWL changes for monitoring groundwater hydrology on inter-annual timescales but cannot directly be related to precipitation.

The seismic station used in this study is located in northern part of the Hockley salt mine at a depth of 413 m (Albuquerque Seismological Laboratory, 1988). Though the geologic condition in the salt mine is likely to be extremely dry, the effective zone of sensitivity of our seismic observables based on autocorrelation kernels (Pacheco & Snieder, 2005) shown in Figure S4 is sufficiently large to ensure ample sensitivity to groundwater changes outside the salt dome (Deussen & Lane, 1925).

To relate GWL to changes in the seismic response of the subsurface, we construct a simple physical model. Figure 4a illustrates a schematic model for GCAS (Figure 2), with the uppermost 500-m layer having an effective porosity of 0.23 (Noble et al., 1996). To relate the effective elastic moduli of the aquifer to the properties of its constituents (e.g., a simplest model with porous aquifer rock, air, and water), we use the fluid substitution approach (Gassmann, 1951) of aquifer rock and the pores with water and air, varying the water level from 0 to 500 m (capturing both high and low GWL scenarios for the GCAS). GWL changes induce correlated changes in  $V_p$ , but anticorrelated, much smaller-amplitude changes in  $V_s$ , regardless of the assumed porosity (Figures 4b and S5). Note that the actual data shown in Figure 3 are sensitive to GWL changes on the order of 15 m and the corresponding prediction for  $V_p$  and  $V_s$  changes are on the order of 1 and 0.1%, respectively. Previous studies have used empirically determined scaling factors to relate GWL changes to  $V_s$  variations (Clements & Denolle, 2018); our physical model, though simple, offers a way of inferring GWL variations from  $V_p$  and/or  $V_s$  changes, if the porosity of the aquifer is known. The function predicting GWL variations from  $V_p$  and/or  $V_s$  changes is specified in the supporting information and shown in Figure S5.

Temporal variations in PSD of RFs do not directly constrain the depth extent of the velocity perturbation (Audet, 2010). However, we find that the correlations between PSD of RFs and GWL depend strongly on frequency (Figure 3b). Using synthetic RFs computed with the wavenumber integration method (Herrmann, 2013), we investigate the frequency-dependent response of RF variations expected for our proposed physical model. We find that GWL changes affect the first 10 s of the synthetic RFs, which are shown in Figure 4c labeled according to the path of the corresponding seismic waves. Though subtle when plotted in time (Figure 4c), RF changes become readily apparent in the PSD (Figure 4d), which show that their sensitivity to time-varying velocity perturbations depends on frequency (depth), with largest variations in the 0.25–0.35 Hz frequency range. The median PSD of synthetic RFs in this range is shown as a dashed line in black and perfectly tracks changes in GWL (Figure 3c).

The relationship between GWL and  $dv/v$  reported here is opposite in sign to that found by Clements & Denolle (2018) using cross-correlations in the San Gabriel Valley, CA. We attribute this difference to the fact that inter-station correlations are more sensitive to S-wave rather than P-wave velocities, because they are dominated by Rayleigh wave energy. Our simple physical model predicts that GWL increase should decrease  $V_s$ , though the relative change in  $V_s$  is lesser by a factor of 10 than that in  $V_p$  (Figures 4b and S5). This is indeed what has been observed: Clements and Denolle (2018) report that a 16.8-m GWL increase decreased  $V_s$  by 0.125% while we find that a 15-m GWL increase increased  $V_p$  by 1.2%. Differences in velocity variations inferred by autocorrelation of horizontal versus vertical component also support the higher sensitivity of  $V_p$  to GWL changes, compared to  $V_s$  (Figure S1). Additional constraints may be provided by analysis of single-station cross-component correlations (Galetti & Curtis, 2012).

As noted, our result from southern Texas does not show a strong correlation with precipitation alone (Figure S1). While a short-lived subsidence signal is observed from GPS after a severe rainfall during hurricane Harvey 2017 (Milliner et al., 2018), its corresponding seismic signature (due to aquifer recharge) is difficult to detect (Figure 3), consistent with the lack of a dramatic increase in GWL recorded at the monitoring well. In order to assess whether the findings presented here for station HKT and the GCAS are likely to be applicable in other geologic settings, we have repeated the analysis at station DWPF in Florida (Figures S6

and S7) and found very similar levels of correlation among  $dv/v$ , RF PSDs, and GWL. Different sensitivities to the distribution of water with depth using seismic and geodetic data thus lend itself to joint inversion in the framework of a groundwater recharge model, opening the door for constraining what fraction of extreme rainfall goes into recharging the groundwater. Because of the wide geographic availability of seismic and geodetic data, such an approach can enable the mapping of key hydraulic parameters including porosity and hydraulic conductivity.

### Acknowledgments

This work is supported by a Packard Foundation Fellowship to V. L. Authors acknowledge the thorough and thoughtful reviews of Dr. Pascal Audet and an anonymous reviewer that greatly improved the manuscript. Authors also thank Mong-Han Huang and Karen Prestegard for insightful discussions. Seismic data in this manuscript are available through IRIS (Incorporated Research Institution for Seismology) Data Management Center (DMC) at network code IU. Seismic observables (receiver functions—both data and synthetics and ambient noise correlation data) produced in this study are available at Digital Repository at the University of Maryland (DRUM; <https://drum.lib.umd.edu/handle/1903/25258>). Groundwater and precipitation data are open and available at USGS National Water Information System (<https://waterdata.usgs.gov/nwis/gw>) and Harris County Flood Warning System (<https://www.harriscountyfws.org>), respectively.

### References

- Abt, D. L., Fischer, K. M., French, S. W., Ford, H. A., Yuan, H., & Romanowicz, B. (2010). North American lithospheric discontinuity structure imaged by Ps and Sp receiver functions. *Journal of Geophysical Research*, 115, B09301. <https://doi.org/10.1029/2009JB006914>
- Albuquerque Seismological Laboratory (ASL)/USGS (1988). Global Seismograph Network (GSN – IRIS/USGS). International Federation of Digital Seismograph Networks. Dataset/Seismic Network. <https://doi.org/10.7914/SN/IU>
- Amelung, F., Galloway, D. L., Bell, J. W., Zebker, H. A., & Lacziak, R. J. (1999). Sensing the ups and downs of Las Vegas: InSAR reveals structural control of land subsidence and aquifer-system deformation. *Geology*, 27(6), 483–486. [https://doi.org/10.1130/0091-7613\(1999\)027<0483:STUADO>2.3.CO;2](https://doi.org/10.1130/0091-7613(1999)027<0483:STUADO>2.3.CO;2)
- Amos, C. B., Audet, P., Hammond, W. C., Bürgmann, R., Johanson, I. A., & Blewitt, G. (2014). Uplift and seismicity driven by groundwater depletion in central California. *Nature*, 509(7501), 483. <https://doi.org/10.1038/nature13275>
- Argus, D. F., Fu, Y., & Landauer, F. W. (2014). Seasonal variation in total water storage in California inferred from GPS observations of vertical land motion. *Geophysical Research Letters*, 41, 1971–1980. <https://doi.org/10.1002/2014GL059570>
- Audet, P. (2010). Temporal variations in crustal scattering structure near Parkfield, California, using receiver functions. *Bulletin of the Seismological Society of America*, 100(3), 1356–1362. <https://doi.org/10.1785/0120090299>
- Baker Jr, E. T. (1979). Stratigraphic and hydrogeologic framework of part of the coastal plain of Texas. Texas Department of Water Resources. <https://hdl.handle.net/1969.3/19363>
- Blakely, R. J. (1995). *Potential theory in gravity and magnetic applications* (p. 441). USA: Cambridge University Press. <https://doi.org/10.1017/CBO9780511549816>
- Borsa, A. A., Agnew, D. C., & Cayan, D. R. (2014). Ongoing drought-induced uplift in the western United States. *Science*, 345(6204), 1587–1590. <https://doi.org/10.1126/science.1260279>
- Brenguier, F., Campillo, M., Hadzioannou, C., Shapiro, N. M., Nadeau, R. M., & Larose, E. (2008). Postseismic relaxation along the San Andreas fault at Parkfield from continuous seismological observations. *Science*, 321(5895), 1478–1481. <https://doi.org/10.1126/science.1160943>
- Burdick, L. J., & Langston, C. A. (1977). Modeling crustal structure through the use of converted phases in teleseismic body-wave forms. *Bulletin of the Seismological Society of America*, 67(3), 677–691.
- Chaussard, E., Milillo, P., Bürgmann, R., Perissin, D., Fielding, E. J., & Baker, B. (2017). Remote sensing of ground deformation for monitoring groundwater management practices: Application to the Santa Clara Valley during the 2012–2015 California drought. *Journal of Geophysical Research: Solid Earth*, 122, 8566–8582. <https://doi.org/10.1002/2017JB014676>
- Chen, J., Famiglietti, J. S., Scanlon, B. R., & Rodell, M. (2016). Groundwater storage changes: Present status from GRACE observations. *Surveys in Geophysics*, 37(2), 397–417. [https://doi.org/10.1007/978-3-319-32449-4\\_9](https://doi.org/10.1007/978-3-319-32449-4_9)
- Clements, T., & Denolle, M. A. (2018). Tracking groundwater levels using the ambient seismic field. *Geophysical Research Letters*, 45, 6459–6465. <https://doi.org/10.1029/2018GL077706>
- Deussen, A., & Lane, L. L. (1925). Hockley salt dome, Harris County, Texas. *AAPG Bulletin*, 9(7), 1031–1060. <https://doi.org/10.1306/3D932EE-16B1-11D7-8645000102C1865D>
- Duputel, Z., Ferrazzini, V., Brenguier, F., Shapiro, N., Campillo, M., & Nercessian, A. (2009). Real time monitoring of relative velocity changes using ambient seismic noise at the Piton de la Fournaise volcano (La Réunion) from January 2006 to June 2007. *Journal of Volcanology and Geothermal Research*, 184(1–2), 164–173. <https://doi.org/10.1016/j.jvolgeores.2008.11.024>
- Duvall, T. L. Jr., Jefferies, S. M., Harvey, J. W., & Pomerantz, M. A. (1993). Time-distance helioseismology. *Nature*, 362(6419), 430. <https://doi.org/10.1038/362430a0>
- Famiglietti, J. S. (2014). The global groundwater crisis. *Nature Climate Change*, 4(11), 945. <https://doi.org/10.1038/nclimate2425>
- Galetti, E., & Curtis, A. (2012). Generalised receiver functions and seismic interferometry. *Tectonophysics*, 532, 1–26. <https://doi.org/10.1016/j.tecto.2011.12.004>
- Gassmann, F. (1951). Elastic waves through a packing of spheres. *Geophysics*, 16(4), 673–685. <https://doi.org/10.1190/1.1437718>
- Goodling, P. J., Lekic, V., & Prestegard, K. (2018). Seismic signature of turbulence during the 2017 Oroville Dam spillway erosion crisis. *Earth Surface Dynamics*, 6(2), 351. <https://doi.org/10.5194/esurf-6-351-2018>
- Hadzioannou, C., Larose, E., Coutant, O., Roux, P., & Campillo, M. (2009). Stability of monitoring weak changes in multiply scattering media with ambient noise correlation: Laboratory experiments. *The Journal of the Acoustical Society of America*, 125(6), 3688–3695. <https://doi.org/10.1121/1.3125345>
- Herrmann, R. B. (2013). Computer programs in seismology: An evolving tool for instruction and research. *Seismological Research Letters*, 84, 1081–1088. <https://doi.org/10.1785/0220110096>
- Huang, M.-H., Bürgmann, R., & Hu, J.-C. (2016). Fifteen years of surface deformation in Western Taiwan: Insight from SAR interferometry. *Tectonophysics*, 692, 252–264. <https://doi.org/10.1016/j.tecto.2016.02.021>
- Kasmarek, M. C., Johnson, M. R., & Ramage, J. K. (2012). *Water-level altitudes 2012 and water-level changes in the Chicot, Evangeline, and Jasper aquifers and compaction 1973–2011 in the Chicot and Evangeline aquifers, Houston-Galveston region*. Texas: US Geological Survey. <https://doi.org/10.3133/sim3230>
- Kasmarek, M. C., & Robinson, J. L. (2004). Hydrogeology and simulation of ground-water flow and land-surface subsidence in the northern part of the Gulf Coast Aquifer System, Texas. US Geological Survey. <https://doi.org/10.3133/sir20045102>
- Kim, D., Keranen, K., Abers, G., & Brown, L. D. (2019). Enhanced resolution of the subducting plate interface in Central Alaska from autocorrelation of local earthquake coda. *Journal of Geophysical Research: Solid Earth*, 124, 1583–1600. <https://doi.org/10.1029/2018JB016167>
- Larose, E., Carrière, S., Voisin, C., Bottelin, P., Baillet, L., Guéguen, P., et al. (2015). Environmental seismology: What can we learn on earth surface processes with ambient noise? *Journal of Applied Geophysics*, 116, 62–74. <https://doi.org/10.1016/j.jappgeo.2015.02.001>

- Leahy, G. M., Saltzer, R. L., & Schmedes, J. (2012). Imaging the shallow crust with teleseismic receiver functions. *Geophysical Journal International*, 191(2), 627–636. <https://doi.org/10.1111/j.1365-246X.2012.05615.x>
- Ligorria, J. P., & Ammon, C. J. (1999). Iterative deconvolution and receiver-function estimation. *Bulletin of the Seismological Society of America*, 89(5), 1395–1400.
- Mainsant, G., Larose, E., Brönnimann, C., Jongmans, D., Michoud, C., & Jaboyedoff, M. (2012). Ambient seismic noise monitoring of a clay landslide: Toward failure prediction. *Journal of Geophysical Research*, 117, F01030. <https://doi.org/10.1029/2011JF002159>
- Meier, U., Shapiro, N. M., & Brenguier, F. (2010). Detecting seasonal variations in seismic velocities within Los Angeles basin from correlations of ambient seismic noise. *Geophysical Journal International*, 181(2), 985–996. <https://doi.org/10.1111/j.1365-246X.2010.04550.x>
- Mikael, A., Gueguen, P., Bard, P.-Y., Roux, P., & Langlais, M. (2013). The analysis of long-term frequency and damping wandering in buildings using the Random Decrement Technique. *Bulletin of the Seismological Society of America*, 103(1), 236–246. <https://doi.org/10.1785/0120120048>
- Milliner, C. W. D., Materna, K., Bürgmann, R., Fu, Y., Bekaert, D., Moore, A., et al. (2018). Tracking the weight of Hurricane Harvey's stormwaters using GPS data. *Science Advances*, 4(9), eaau2477. <https://doi.org/10.1126/sciadv.aau2477>
- Mordret, A., Mikesell, T. D., Harig, C., Lipovsky, B. P., & Prieto, G. A. (2016). Monitoring southwest Greenland's ice sheet melt with ambient seismic noise. *Science Advances*, 2(5), e1501538. <https://doi.org/10.1126/sciadv.1501538>
- Niu, F., Silver, P. G., Daley, T. M., Cheng, X., & Majer, E. L. (2008). Preseismic velocity changes observed from active source monitoring at the Parkfield SAFOD drill site. *Nature*, 454(7201), 204–208. <https://doi.org/10.1038/nature07111>
- Noble, J. E., Bush, P. W., Kasmarek, M. C., & Barbie, D. L. (1996). *Estimated depth to the water table and estimated rate of recharge in outcrops of the Chicot and Evangeline aquifers near Houston*. Texas: US Geological Survey. <https://doi.org/10.3133/wri964018>
- Pacheco, C., & Snieder, R. (2005). Time-lapse travel time change of multiply scattered acoustic waves. *The Journal of the Acoustical Society of America*, 118(3), 1300–1310. <https://doi.org/10.1121/1.2000827>
- Porritt, R. W., & Yoshioka, S. (2017). Evidence of dynamic crustal deformation in Tohoku, Japan, from time-varying receiver functions. *Tectonics*, 36, 1934–1946. <https://doi.org/10.1002/2016TC004413>
- Poupinet, G., Ellsworth, W. L., & Frechet, J. (1984). Monitoring velocity variations in the crust using earthquake doublets: An application to the Calaveras Fault, California. *Journal of Geophysical Research*, 89(B7), 5719–5731. <https://doi.org/10.1029/JB089iB07p05719>
- Rodell, M., Chen, J., Kato, H., Famiglietti, J. S., Nigro, J., & Wilson, C. R. (2007). Estimating groundwater storage changes in the Mississippi River basin (USA) using GRACE. *Hydrogeology Journal*, 15(1), 159–166. <https://doi.org/10.1007/s10040-006-0103-7>
- Rodell, M., Velicogna, I., & Famiglietti, J. S. (2009). Satellite-based estimates of groundwater depletion in India. *Nature*, 460(7258), 999–1002. <https://doi.org/10.1038/nature08238>
- Schmandt, B., Aster, R. C., Scherler, D., Tsai, V. C., & Karlstrom, K. (2013). Multiple fluvial processes detected by riverside seismic and infrasound monitoring of a controlled flood in the Grand Canyon. *Geophysical Research Letters*, 40, 4858–4863. <https://doi.org/10.1002/grl.50953>
- Schmidt, D. A., & Bürgmann, R. (2003). Time-dependent land uplift and subsidence in the Santa Clara valley, California, from a large interferometric synthetic aperture radar data set. *Journal of Geophysical Research*, 108(B9), 2416. <https://doi.org/10.1029/2002JB002267>
- Sens-Schönfelder, C., & Larose, E. (2008). Temporal changes in the lunar soil from correlation of diffuse vibrations. *Physical Review E*, 78(4), 45601. <https://doi.org/10.1103/PhysRevE.78.045601>
- Sens-Schönfelder, C., & Wegler, U. (2006). Passive image interferometry and seasonal variations of seismic velocities at Merapi Volcano, Indonesia. *Geophysical Research Letters*, 33, L21302. <https://doi.org/10.1029/2006GL027797>
- Sens-Schönfelder, C., & Wegler, U. (2011). Passive image interferometry for monitoring crustal changes with ambient seismic noise. *Comptes Rendus Geoscience*, 343(8–9), 639–651. <https://doi.org/10.1016/j.crte.2011.02.005>
- Shapiro, N. M., Campillo, M., Stehly, L., & Ritzwoller, M. H. (2005). High-resolution surface-wave tomography from ambient seismic noise. *Science*, 307(5715), 1615–1618. <https://doi.org/10.1126/science.1108339>
- Silver, P. G., Daley, T. M., Niu, F., & Majer, E. L. (2007). Active source monitoring of cross-well seismic travel time for stress-induced changes. *Bulletin of the Seismological Society of America*, 97(1B), 281–293. <https://doi.org/10.1785/0120060120>
- Snieder, R., & Page, J. (2007). Multiple scattering in evolving media. *Physics Today*, 60(5), 49. <https://doi.org/10.1063/1.2743124>
- Strassberg, G., Scanlon, B. R., & Rodell, M. (2007). Comparison of seasonal terrestrial water storage variations from GRACE with groundwater-level measurements from the High Plains Aquifer (USA). *Geophysical Research Letters*, 34, L14402. <https://doi.org/10.1029/2007GL030139>
- Swenson, S., Yeh, P. J.-F., Wahr, J., & Famiglietti, J. (2006). A comparison of terrestrial water storage variations from GRACE with in situ measurements from Illinois. *Geophysical Research Letters*, 33, L16401. <https://doi.org/10.1029/2006GL026962>
- Tsai, V. C. (2011). A model for seasonal changes in GPS positions and seismic wave speeds due to thermoelastic and hydrologic variations. *Journal of Geophysical Research*, 116, B04404. <https://doi.org/10.1029/2010JB008156>
- U.S. Geological Survey (2016). National Water Information System data available on the World Wide Web (USGS Water Data for the Nation). <http://doi.org/10.5066/F7P55KJN>
- Ventosa, S., Schimmel, M., & Stutzmann, E. (2017). Extracting surface waves, hum and normal modes: Time-scale phase-weighted stack and beyond. *Geophysical Journal International*, 211(1), 30–44. <https://doi.org/10.1093/gji/ggx284>
- Wada, Y., van Beek, L. P., van Kempen, C. M., Reckman, J. W., Vasak, S., & Bierkens, M. F. (2010). Global depletion of groundwater resources. *Geophysical Research Letters*, 37, L20402. <https://doi.org/10.1029/2010GL044571>
- Wegler, U., Nakahara, H., Sens-Schönfelder, C., Korn, M., & Shiomi, K. (2009). Sudden drop of seismic velocity after the 2004  $M_w$  6.6 mid-Niigata earthquake, Japan, observed with Passive Image Interferometry. *Journal of Geophysical Research*, 114, B06305. <https://doi.org/10.1029/2008JB005869>
- Wegler, U., & Sens-Schönfelder, C. (2007). Fault zone monitoring with passive image interferometry. *Geophysical Journal International*, 168(3), 1029–1033. <https://doi.org/10.1111/j.1365-246X.2006.03284.x>
- Yeh, P. J.-F., Swenson, S. C., Famiglietti, J. S., & Rodell, M. (2006). Remote sensing of groundwater storage changes in Illinois using the Gravity Recovery and Climate Experiment (GRACE). *Water Resources Research*, 42, W12203. <https://doi.org/10.1029/2006WR005374>